Neurobasal medium (Gibco) and then incubated for 5 min on ice. After removing the supernatant, 5 ml of Neurobasal medium was added, followed by a further 5-min incubation on ice. The cells were then incubated in Hanks' balanced salt solutions (HBSS, Gibco) containing 0.25% trypsin for 15 min at 37°C. DNase I (final 0.05%) was added, and the cells were incubated for 1 min at 37°C. After pipetting ten times and centrifugation, the cell pellet was suspended and incubated in HBSS containing 0.05% DNase I for 3 min at 37°C. The cells were centrifuged and resuspended in complete culture medium (Neurobasal medium supplemented with 2% B27 and 0.5 mM glutamine) and passed through a 100-μm strainer. They were then seeded at 5×10^5 or 2.5×10^5/ml per dish or chamber slide which had been precoated with poly-D-lysine. After 2 days, Ara-C (C6645, Sigma) was added at 5 μM to kill dividing non-neuronal cells.

Lentiviral infection

To produce the lentiviral vector, 293FT cells plated in 10-cm dishes were simultaneously transfected with 2.25 μg of pLP1, 2.25 μg of pLP2, 4.5 μg of pLP/VSVG, and 3 μg of pLenti6/human BACE1 using Lipofectamine 2000. The following day, the medium was replaced with fresh medium, and after 48 h (72 h post-transfection), the medium was collected. Cells and debris were removed by centrifugation, and the medium was passed through a filter (pore size 0.45 μm). The viruses were collected by centrifugation at 50,000 × *g* for 2 h at 20°C and then resuspended in Neurobasal medium to concentrate the viruses (12-fold). The virus solution was directly added to the primary neuron culture medium after 2 days *in vitro*.

Cell culture and transfection

C17, COS-7, and MEF cells were cultured in DMEM supplemented with 10% FBS. For plasmid transfection, cells at 80% confluency on a 10-cm dish were transfected with 4–8 μg of each plasmid using 10–20 μl of Lipofectamine 2000 (for COS-7 cells).

siRNA treatment

For knockdown experiments, FlexiTube siRNAs (Qiagen) were used. MEFs at 30% confluency on 10-cm (or 6-cm) dishes were transfected with 200 pmol (or 80 pmol) of control siRNA (AllStars negative control siRNA, Qiagen) or siRNA for GGA3 (SI01011451) using 20 μl (or 8 μl) of Lipofectamine 2000. At 24 h or 48 h after transfection, cells were used for other experiments.

Subcellular fractionation by sucrose density gradient centrifugation

Subcellular fractionation was performed as described previously (Aniento *et al*, 1993) with modifications. All the buffers contained 20 mM Tris–HCl pH 7.5 and 3 mM imidazole. Cells were homogenized with buffer containing 8.5% sucrose and protease inhibitor cocktail by passaging 10 times through a 26-gauge needle. After removal of nuclei and debris by centrifugation at 1,000 × *g* for 5 min, the concentration of sucrose was adjusted to 40.6%. The sample (1 ml) was loaded at the bottom of a tube and overlaid with 1 ml of 35% sucrose, 1 ml of 25% sucrose, and 1 ml of the homogenization buffer. After ultracentrifugation using an S52ST rotor at 150,000 × *g* for 90 min, interfaces at 8.5/25, 25/35, and 35/40.6% were recovered. To sediment membranes, the collected samples were diluted fourfold and then ultracentrifuged at 180,000 × *g* for 30 min. The resultant pellets were solubilized, and protein concentrations were measured. An equivalent amount of protein was taken from each fraction for Western blotting. In the case of mouse brains, the whole brain was first homogenized with seven volumes of the same buffer containing 8.5% sucrose, after which the nuclei and debris were removed. The postnuclear solution was adjusted to 40.6% sucrose, and 1 ml of the sample was loaded at the tube and overlaid with 1 ml of 35% sucrose, 1 ml of 30% sucrose, and 1 ml of 25% sucrose solutions. After ultracentrifugation using a S52ST rotor at 100,000 × *g* for 90 min, the top fraction and interfaces at 25/30, 30/35, and 35/40.6% were collected. For separation of 11 fractions, a previously described method (Tan *et al*, 2013) was modified. 1 ml of 44.5% sucrose was loaded in the tube and overlaid with 3 ml of 39.7% sucrose, 3 ml of 34.2% sucrose, 3 ml of 27.4% sucrose, and 1 ml of the postnuclear solution. After ultracentrifugation using P40ST rotor at 120,000 × *g* for 16 h, each fraction (1 ml) was collected. Equal volumes of the fractions were used for Western blotting.

RNA extraction, reverse-transcription and quantitative PCR

Total RNA from cultured cells was extracted using TRIzol (Invitrogen). One microgram of total RNA was reverse-transcribed using the SuperScript III First-Strand Synthesis System (Invitrogen) with random hexamers. For BACE1 primers and probe, we used Assays-on-Demand gene expression products, and cDNAs were added to the TaqMan Universal PCR Master Mix (Applied Biosystems). The probe for BACE1 was labeled with FAM at its 5′-end and with the quencher MGB at its 3′-end. The probes for rRNA were labeled with VIC at their 5′-end and with the quencher TAMRA at their 3′-end. The cDNAs were amplified using an ABI PRISM 7900HT sequence detection system (Applied Biosystems). The level of BACE1 mRNA was measured in duplicate and normalized to the corresponding rRNA level.

Human samples

The clinical study was approved by the ethical committees of RIKEN, Tokyo Metropolitan Institute of Gerontology, and Tokyo Metropolitan Geriatric Hospital. Frozen tissues from postmortem brain were obtained from the Brain Bank for Aging Research, which consists of consecutive autopsy cases from a general geriatric hospital with informed consent obtained from the relatives for each autopsy. Handling of the brains and diagnostic criteria have been described previously (Akasaka-Manya *et al*, 2010). One gram of temporal pole tissue was sampled from 10 cases each with AD or early AD, and age-matched controls (the same cases as reported in the previous study(Akasaka-Manya *et al*, 2010)). A summary of the clinical and histological data is shown in Fig 2A. The brains were homogenized with five volumes of buffer (20 mM Tris–HCl, pH 7.4, 150 mM NaCl, 5 mM EDTA, and protease inhibitor cocktail) using stainless steel beads (7.9 mm) in Micro Smash (TOMY) for 40 (1^{st}) and 20 (2^{nd}) seconds at 3,500 rpm. The homogenates were

ultracentrifuged at 100,000 × *g* for 1 h to obtain membrane fractions. BACE1 immunoprecipitation and Western blotting were carried out (no blinding) as described above for mouse brain with slight modifications. We used magnetic Dynabeads protein G for protein pulldown. The lysates were first pre-cleared by the beads in the absence of antibody addition.

Construction of a three-dimensional model of *N*-glycosylated human BACE1

A 3D structural model of human BACE1 with bisected *N*-glycans was generated by GlyProt (Bohne-Lang & von der Lieth, 2005). The atomic coordinate of unglycosylated human BACE1 (PDB code: 2qp8) was used for the construction of the glycosylated model (Shimizu *et al*, 2008), and the bisected *N*-glycans ($GlcNAc_1Man_3GlcNAc_2$) were attached to four *N*-glycosylation sites, Asn153, Asn172, Asn223, and Asn354.

Statistical analysis

All data are shown as mean ± SEM. For comparison of the means between two groups, statistical analysis was performed by applying an unpaired one-sided Student's *t*-test after confirming equality between two groups and normality by a Kolmogorov–Smirnov test. If these tests were not passed, a Mann–Whitney *U*-test was performed. Comparisons of the means among more than two groups were done by a one-way or two-way analysis of variance (ANOVA) followed by a *post hoc* test, in which a Student–Newman–Keuls test (SigmaPlot software, ver.11; Systat Software Inc.) or Tukey–Kramer test was applied. *P*-values < 0.05 were considered to be significant.

Supplementary information for this article is available online: http://embomolmed.embopress.org

Acknowledgements
We thank Dr. Keiko Akasaka (Tokyo Metropolitan Geriatric Hospital and Institute of Gerontology) and Ms. Keiko Sato (RIKEN) for technical help. *Mgat3*-deficient mice were generously provided by Dr. Jamey D. Marth (University of California-Santa Barbara). We also thank the staff of RIKEN BSI Research Resources Center for chemical synthesis of BACE1 C-terminal peptide (the Support Unit for Bio-Material Analysis) and for the Y-maze test (Support Unit for Animal Resources Development). This work was supported by RIKEN (the Systems Glycobiology Research project to NT, Special Postdoctoral Researchers Program to YK, and Incentive Research Grant to YK) and by the Japan Society for the Promotion of Science (JSPS) (Grant-in-Aid for Scientific Research (A) to NT and for Scientific Research on Innovative Areas to HM).

Author contributions
YK, SK, and NT designed the experiments and wrote the manuscript. YK performed most of the biochemical and cell biological experiments. RF prepared the mutant mice and conducted the biochemical analysis. MN carried out mass spectrometric analyses. HH, SM, and HM prepared and analyzed the human samples. YY performed the computational modeling. YK, SK, TS, NI, TCS, YY, YH, MS, HM, TE, and NT interpreted the data.

Conflict of interest
The authors declare that they have no conflict of interest.

The paper explained

Problem
Alzheimer's disease (AD) is the most common dementia and is a serious issue in aging populations throughout the world. However, efforts to develop therapeutic agents for AD have so far achieved limited success. The deposition of amyloid β (Aβ) peptide in the brain, resulting in Aβ plaques, is the biochemical hallmark of AD. Currently, one of the most promising targets for AD therapy is the enzyme BACE1 (β-site amyloid precursor protein cleaving enzyme-1), which generates Aβ from its precursor protein. Several BACE1 inhibitors are in clinical trials, but there is a concern about side effects, given that BACE1 also cleaves other proteins in the brain. Indeed, *Bace1* knockout mice exhibit severe phenotypes such as schizophrenia-like symptoms, muscle abnormality, retinal pathology, and early lethality. Therefore, modulation of BACE1 function with fewer detrimental side effects would be a rational and promising strategy to ameliorate AD pathology. However, little is known about the regulation of BACE1 function at the level of cellular expression and compartmental localization during health and disease.

Results
In this study, we show that a unique sugar modification, 'bisecting GlcNAc', on BACE1 is a novel regulator of cellular BACE1 stability. We found that BACE1 is abnormally modified, with higher levels of bisecting GlcNAc being observed in AD patients, suggesting the pathological involvement of this sugar modification on BACE1 during AD development. Using AD model mice and knockout mice lacking the glycosyl enzyme (GnT-III) responsible for the biosynthesis of bisecting GlcNAc, we demonstrated that the loss of bisecting GlcNAc diminishes Aβ plaque formation by reducing BACE1-mediated Aβ generation. The decrease in Aβ generation in the knockout mice was caused by a shift in the intracellular distribution of BACE1 from early endosomes (where Aβ precursor protein is localized) to late endosomes/lysosomes, leading to faster lysosomal degradation of BACE1. These results indicate that bisecting GlcNAc is a novel pathological modification of BACE1 which delays its degradation.

Impact
Knockout mice for bisecting GlcNAc exhibit a robust reduction in Aβ production but show almost no abnormality in contrast to the severe phenotypes of *Bace1* knockout mice. The latter phenotypes are caused by the impaired cleavage of physiological BACE1 substrates, whereas we found that a BACE1 substrate other than Aβ-precursor protein is normally cleaved in GnT-III-deficient mice, suggesting that the inhibitory effects of bisecting GlcNAc on BACE1 are selective to the Aβ-generation pathway. Therefore, inhibiting the biosynthesis of bisecting GlcNAc could block the AD-related pathological effect of BACE1, while having only weak detrimental effects on normal physiological BACE1 functions. These findings suggest that the biosynthetic pathway for bisecting GlcNAc could serve as a novel and promising drug target for AD therapy, resulting in fewer side effects than BACE1 inhibitors.

References

Abbott A (2011) Dementia: a problem for our age. *Nature* 475: S2–S4

Akasaka-Manya K, Manya H, Sakurai Y, Wojczyk BS, Spitalnik SL, Endo T (2008) Increased bisecting and core-fucosylated N-glycans on mutant human amyloid precursor proteins. *Glycoconj J* 25: 775–786

Akasaka-Manya K, Manya H, Sakurai Y, Wojczyk BS, Kozutsumi Y, Saito Y, Taniguchi N, Murayama S, Spitalnik SL, Endo T (2010) Protective effect of N-glycan bisecting GlcNAc residues on beta-amyloid production in Alzheimer's disease. *Glycobiology* 20: 99–106

Aniento F, Emans N, Griffiths G, Gruenberg J (1993) Cytoplasmic dynein-dependent vesicular transport from early to late endosomes. *J Cell Biol* 123: 1373 – 1387

von Arnim CA, Kinoshita A, Peltan ID, Tangredi MM, Herl L, Lee BM, Spoelgen R, Hshieh TT, Ranganathan S, Battey FD, *et al* (2005) The low density lipoprotein receptor-related protein (LRP) is a novel beta-secretase (BACE1) substrate. *J Biol Chem* 280: 17777 – 17785

Bhattacharyya R, Bhaumik M, Raju TS, Stanley P (2002) Truncated, inactive N-acetylglucosaminyltransferase III (GlcNAc-TIII) induces neurological and other traits absent in mice that lack GlcNAc-TIII. *J Biol Chem* 277: 26300 – 26309

Bohne-Lang A, von der Lieth CW (2005) GlyProt: in silico glycosylation of proteins. *Nucleic Acids Res* 33: W214 – W219

Cai J, Qi X, Kociok N, Skosyrski S, Emilio A, Ruan Q, Han S, Liu L, Chen Z, Bowes Rickman C, *et al* (2012) Beta-Secretase (BACE1) inhibition causes retinal pathology by vascular dysregulation and accumulation of age pigment. *EMBO Mol Med* 4: 980 – 991

Cheret C, Willem M, Fricker FR, Wende H, Wulf-Goldenberg A, Tahirovic S, Nave KA, Saftig P, Haass C, Garratt AN, *et al* (2013) Bace1 and Neuregulin-1 cooperate to control formation and maintenance of muscle spindles. *EMBO J* 32: 2015 – 2028

Cummings RD, Kornfeld S (1982) Characterization of the structural determinants required for the high affinity interaction of asparagine-linked oligosaccharides with immobilized Phaseolus vulgaris leukoagglutinating and erythroagglutinating lectins. *J Biol Chem* 257: 11230 – 11234

Das U, Scott DA, Ganguly A, Koo EH, Tang Y, Roy S (2013) Activity-induced convergence of APP and BACE-1 in acidic microdomains via an endocytosis-dependent pathway. *Neuron* 79: 447 – 460

De Strooper B, Annaert W (2010) Novel research horizons for presenilins and gamma-secretases in cell biology and disease. *Annu Rev Cell Dev Biol* 26: 235 – 260

De Strooper B, Saftig P, Craessaerts K, Vanderstichele H, Guhde G, Annaert W, Von Figura K, Van Leuven F (1998) Deficiency of presenilin-1 inhibits the normal cleavage of amyloid precursor protein. *Nature* 391: 387 – 390

Dennis JW, Nabi IR, Demetriou M (2009) Metabolism, cell surface organization, and disease. *Cell* 139: 1229 – 1241

Dominguez D, Tournoy J, Hartmann D, Huth T, Cryns K, Deforce S, Serneels L, Camacho IE, Marjaux E, Craessaerts K, *et al* (2005) Phenotypic and biochemical analyses of BACE1- and BACE2-deficient mice. *J Biol Chem* 280: 30797 – 30806

Eggert S, Paliga K, Soba P, Evin G, Masters CL, Weidemann A, Beyreuther K (2004) The proteolytic processing of the amyloid precursor protein gene family members APLP-1 and APLP-2 involves alpha-, beta-, gamma-, and epsilon-like cleavages: modulation of APLP-1 processing by n-glycosylation. *J Biol Chem* 279: 18146 – 18156

Fiala M, Liu PT, Espinosa-Jeffrey A, Rosenthal MJ, Bernard G, Ringman JM, Sayre J, Zhang L, Zaghi J, Dejbakhsh S, *et al* (2007) Innate immunity and transcription of MGAT-III and Toll-like receptors in Alzheimer's disease patients are improved by bisdemethoxycurcumin. *Proc Natl Acad Sci USA* 104: 12849 – 12854

Fiala M, Mahanian M, Rosenthal M, Mizwicki MT, Tse E, Cho T, Sayre J, Weitzman R, Porter V (2011) MGAT3 mRNA: a biomarker for prognosis and therapy of Alzheimer's disease by vitamin D and curcuminoids. *J Alzheimers Dis* 25: 135 – 144

Godfrey C, Foley AR, Clement E, Muntoni F (2011) Dystroglycanopathies: coming into focus. *Curr Opin Genet Dev* 21: 278 – 285

Hebert DN, Garman SC, Molinari M (2005) The glycan code of the endoplasmic reticulum: asparagine-linked carbohydrates as protein maturation and quality-control tags. *Trends Cell Biol* 15: 364 – 370

Herreman A, Van Gassen G, Bentahir M, Nyabi O, Craessaerts K, Mueller U, Annaert W, De Strooper B (2003) gamma-Secretase activity requires the presenilin-dependent trafficking of nicastrin through the Golgi apparatus but not its complex glycosylation. *J Cell Sci* 116: 1127 – 1136

Hitt B, Riordan SM, Kukreja L, Eimer WA, Rajapaksha TW, Vassar R (2012) beta-Site amyloid precursor protein (APP)-cleaving enzyme 1 (BACE1)-deficient mice exhibit a close homolog of L1 (CHL1) loss-of-function phenotype involving axon guidance defects. *J Biol Chem* 287: 38408 – 38425

Hu X, Hicks CW, He W, Wong P, Macklin WB, Trapp BD, Yan R (2006) Bace1 modulates myelination in the central and peripheral nervous system. *Nat Neurosci* 9: 1520 – 1525

Ihara H, Ikeda Y, Koyota S, Endo T, Honke K, Taniguchi N (2002) A catalytically inactive beta 1,4-N-acetylglucosaminyltransferase III (GnT-III) behaves as a dominant negative GnT-III inhibitor. *Eur J Biochem* 269: 193 – 201

Iwata N, Mizukami H, Shirotani K, Takaki Y, Muramatsu S, Lu B, Gerard NP, Gerard C, Ozawa K, Saido TC (2004) Presynaptic localization of neprilysin contributes to efficient clearance of amyloid-beta peptide in mouse brain. *J Neurosci* 24: 991 – 998

Kang EL, Cameron AN, Piazza F, Walker KR, Tesco G (2010) Ubiquitin regulates GGA3-mediated degradation of BACE1. *J Biol Chem* 285: 24108 – 24119

Kao SC, Krichevsky AM, Kosik KS, Tsai LH (2004) BACE1 suppression by RNA interference in primary cortical neurons. *J Biol Chem* 279: 1942 – 1949

Karran E, Mercken M, De Strooper B (2011) The amyloid cascade hypothesis for Alzheimer's disease: an appraisal for the development of therapeutics. *Nat Rev Drug Discov* 10: 698 – 712

Kim DY, Ingano LA, Carey BW, Pettingell WH, Kovacs DM (2005) Presenilin/gamma-secretase-mediated cleavage of the voltage-gated sodium channel beta2-subunit regulates cell adhesion and migration. *J Biol Chem* 280: 23251 – 23261

Kitada T, Miyoshi E, Noda K, Higashiyama S, Ihara H, Matsuura N, Hayashi N, Kawata S, Matsuzawa Y, Taniguchi N (2001) The addition of bisecting N-acetylglucosamine residues to E-cadherin down-regulates the tyrosine phosphorylation of beta-catenin. *J Biol Chem* 276: 475 – 480

Kitazume S, Tachida Y, Oka R, Shirotani K, Saido TC, Hashimoto Y (2001) Alzheimer's beta-secretase, beta-site amyloid precursor protein-cleaving enzyme, is responsible for cleavage secretion of a Golgi-resident sialyltransferase. *Proc Natl Acad Sci USA* 98: 13554 – 13559

Kitazume S, Tachida Y, Kato M, Yamaguchi Y, Honda T, Hashimoto Y, Wada Y, Saito T, Iwata N, Saido T, *et al* (2010) Brain endothelial cells produce amyloid beta from amyloid precursor protein 770 and preferentially secrete the O-glycosylated form. *J Biol Chem* 285: 40097 – 40103

Koh YH, von Arnim CA, Hyman BT, Tanzi RE, Tesco G (2005) BACE is degraded via the lysosomal pathway. *J Biol Chem* 280: 32499 – 32504

Kuhn PH, Koroniak K, Hogl S, Colombo A, Zeitschel U, Willem M, Volbracht C, Schepers U, Imhof A, Hoffmeister A, *et al* (2012) Secretome protein enrichment identifies physiological BACE1 protease substrates in neurons. *EMBO J* 31: 3157 – 3168

Li Q, Sudhof TC (2004) Cleavage of amyloid-beta precursor protein and amyloid-beta precursor-like protein by BACE 1. *J Biol Chem* 279: 10542 – 10550

Lichtenthaler SF, Dominguez DI, Westmeyer GG, Reiss K, Haass C, Saftig P, De Strooper B, Seed B (2003) The cell adhesion protein P-selectin glycoprotein

ligand-1 is a substrate for the aspartyl protease BACE1. *J Biol Chem* 278: 48713 – 48719

Luo Y, Bolon B, Kahn S, Bennett BD, Babu-Khan S, Denis P, Fan W, Kha H, Zhang J, Gong Y, *et al* (2001) Mice deficient in BACE1, the Alzheimer's beta-secretase, have normal phenotype and abolished beta-amyloid generation. *Nat Neurosci* 4: 231 – 232

Nakano M, Saldanha R, Gobel A, Kavallaris M, Packer NH (2011) Identification of glycan structure alterations on cell membrane proteins in desoxyepothilone B resistant leukemia cells. *Mol Cell Proteomics* 10: M111 009001

Nishikawa A, Ihara Y, Hatakeyama M, Kangawa K, Taniguchi N (1992) Purification, cDNA cloning, and expression of UDP-N-acetylglucosamine: beta-D-mannoside beta-1, 4N-acetylglucosaminyltransferase III from rat kidney. *J Biol Chem* 267: 18199 – 18204

Ohtsubo K, Takamatsu S, Minowa MT, Yoshida A, Takeuchi M, Marth JD (2005) Dietary and genetic control of glucose transporter 2 glycosylation promotes insulin secretion in suppressing diabetes. *Cell* 123: 1307 – 1321

Orr SL, Le D, Long JM, Sobieszczuk P, Ma B, Tian H, Fang X, Paulson JC, Marth JD, Varki N (2013) A phenotype survey of 36 mutant mouse strains with gene-targeted defects in glycosyltransferases or glycan-binding proteins. *Glycobiology* 23: 363 – 380

Pastorino L, Ikin AF, Lamprianou S, Vacaresse N, Revelli JP, Platt K, Paganetti P, Mathews PM, Harroch S, Buxbaum JD (2004) BACE (beta-secretase) modulates the processing of APLP2 in vivo. *Mol Cell Neurosci* 25: 642 – 649

Priatel JJ, Sarkar M, Schachter H, Marth JD (1997) Isolation, characterization and inactivation of the mouse Mgat3 gene: the bisecting N-acetylglucosamine in asparagine-linked oligosaccharides appears dispensable for viability and reproduction. *Glycobiology* 7: 45 – 56

Saito T, Suemoto T, Brouwers N, Sleegers K, Funamoto S, Mihira N, Matsuba Y, Yamada K, Nilsson P, Takano J, *et al* (2011) Potent amyloidogenicity and pathogenicity of Abeta43. *Nat Neurosci* 14: 1023 – 1032

Saito T, Matsuba Y, Mihira N, Takano J, Nilsson P, Itohara S, Iwata N, Saido TC (2014) Single App knock-in mouse models of Alzheimer's disease. *Nat Neurosci* 17: 661 – 663

Savonenko AV, Melnikova T, Laird FM, Stewart KA, Price DL, Wong PC (2008) Alteration of BACE1-dependent NRG1/ErbB4 signaling and schizophrenia-like phenotypes in BACE1-null mice. *Proc Natl Acad Sci USA* 105: 5585 – 5590

Schedin-Weiss S, Winblad B, Tjernberg LO (2014) The role of protein glycosylation in Alzheimer disease. *FEBS J* 281: 46 – 62

Schmechel A, Strauss M, Schlicksupp A, Pipkorn R, Haass C, Bayer TA, Multhaup G (2004) Human BACE forms dimers and colocalizes with APP. *J Biol Chem* 279: 39710 – 39717

Selkoe DJ (2012) Preventing Alzheimer's disease. *Science* 337: 1488 – 1492

Shimizu H, Tosaki A, Kaneko K, Hisano T, Sakurai T, Nukina N (2008) Crystal structure of an active form of BACE1, an enzyme responsible for amyloid beta protein production. *Mol Cell Biol* 28: 3663 – 3671

Sturchler-Pierrat C, Abramowski D, Duke M, Wiederhold KH, Mistl C, Rothacher S, Ledermann B, Burki K, Frey P, Paganetti PA, *et al* (1997) Two amyloid precursor protein transgenic mouse models with Alzheimer disease-like pathology. *Proc Natl Acad Sci USA* 94: 13287 – 13292

Tan J, Evin G (2012) Beta-site APP-cleaving enzyme 1 trafficking and Alzheimer's disease pathogenesis. *J Neurochem* 120: 869 – 880

Tan JL, Li QX, Ciccotosto GD, Crouch PJ, Culvenor JG, White AR, Evin G (2013) Mild oxidative stress induces redistribution of BACE1 in non-apoptotic conditions and promotes the amyloidogenic processing of Alzheimer's disease amyloid precursor protein. *PLoS ONE* 8: e61246

Taniguchi N, Miyoshi E, Gu J, Honke K, Matsumoto A (2006) Decoding sugar functions by identifying target glycoproteins. *Curr Opin Struct Biol* 16: 561 – 566

Tesco G, Koh YH, Kang EL, Cameron AN, Das S, Sena-Esteves M, Hiltunen M, Yang SH, Zhong Z, Shen Y, *et al* (2007) Depletion of GGA3 stabilizes BACE and enhances beta-secretase activity. *Neuron* 54: 721 – 737

Vassar R, Kuhn PH, Haass C, Kennedy ME, Rajendran L, Wong PC, Lichtenthaler SF (2014) Function, therapeutic potential and cell biology of BACE proteases: current status and future prospects. *J Neurochem* 130: 4 – 28

Walker KR, Kang EL, Whalen MJ, Shen Y, Tesco G (2012) Depletion of GGA1 and GGA3 mediates postinjury elevation of BACE1. *J Neurosci* 32: 10423 – 10437

Wang X, Inoue S, Gu J, Miyoshi E, Noda K, Li W, Mizuno-Horikawa Y, Nakano M, Asahi M, Takahashi M, *et al* (2005) Dysregulation of TGF-beta1 receptor activation leads to abnormal lung development and emphysema-like phenotype in core fucose-deficient mice. *Proc Natl Acad Sci USA* 102: 15791 – 15796

Wen L, Tang FL, Hong Y, Luo SW, Wang CL, He W, Shen C, Jung JU, Xiong F, Lee DH, *et al* (2011) VPS35 haploinsufficiency increases Alzheimer's disease neuropathology. *J Cell Biol* 195: 765 – 779

Westmeyer GG, Willem M, Lichtenthaler SF, Lurman G, Multhaup G, Assfalg-Machleidt I, Reiss K, Saftig P, Haass C (2004) Dimerization of beta-site beta-amyloid precursor protein-cleaving enzyme. *J Biol Chem* 279: 53205 – 53212

Willem M, Garratt AN, Novak B, Citron M, Kaufmann S, Rittger A, DeStrooper B, Saftig P, Birchmeier C, Haass C (2006) Control of peripheral nerve myelination by the beta-secretase BACE1. *Science* 314: 664 – 666

Wong HK, Sakurai T, Oyama F, Kaneko K, Wada K, Miyazaki H, Kurosawa M, De Strooper B, Saftig P, Nukina N (2005) beta Subunits of voltage-gated sodium channels are novel substrates of beta-site amyloid precursor protein-cleaving enzyme (BACE1) and gamma-secretase. *J Biol Chem* 280: 23009 – 23017

Yang LB, Lindholm K, Yan R, Citron M, Xia W, Yang XL, Beach T, Sue L, Wong P, Price D, *et al* (2003) Elevated beta-secretase expression and enzymatic activity detected in sporadic Alzheimer disease. *Nat Med* 9: 3 – 4

Zhou L, Barao S, Laga M, Bockstael K, Borgers M, Gijsen H, Annaert W, Moechars D, Mercken M, Gevaert K, *et al* (2012) The neural cell adhesion molecules L1 and CHL1 are cleaved by BACE1 protease in vivo. *J Biol Chem* 287: 25927 – 25940

nature neuroscience

Single *App* knock-in mouse models of Alzheimer's disease

Takashi Saito[1,2], Yukio Matsuba[1], Naomi Mihira[1], Jiro Takano[1], Per Nilsson[1], Shigeyoshi Itohara[3], Nobuhisa Iwata[1,4] & Takaomi C Saido[1]

Experimental studies of Alzheimer's disease have largely depended on transgenic mice overexpressing amyloid precursor protein (APP). These mice, however, suffer from artificial phenotypes because, in addition to amyloid β peptide (Aβ), they overproduce other APP fragments. We generated knock-in mice that harbor Swedish and Beyreuther/Iberian mutations with and without the Arctic mutation in the *APP* gene. The mice showed typical Aβ pathology, neuroinflammation and memory impairment in an age-dependent manner.

Identification of a protective mutation in the *APP* gene against sporadic Alzheimer's disease (AD)[1] has substantiated the Aβ hypothesis that was originally based on the discovery of gene mutations that cause familial AD[2]. This hypothesis has led to the generation of a number of transgenic (Tg) mouse models that overexpress APP[3,4], but these mice contain intrinsic problems that may induce artificial phenotypes (**Supplementary Table 1** and **Supplementary Fig. 1a**). We overcame these problems by creating simple models that overproduce $A\beta_{42}$ without overexpressing APP.

We manipulated the mouse *App* gene using a knock-in strategy (**Supplementary Figs. 1b** and **2**) using Swedish (KM670/671NL)[5] and Beyreuther/Iberian (I716F) mutations[6,7]. The Swedish mutation elevates the total amount of $A\beta_{40}$ and $A\beta_{42}$, whereas the Beyreuther/Iberian mutation increases the ratio of $A\beta_{42}$ to $A\beta_{40}$. We first humanized the murine Aβ sequence and inserted Swedish mutations (App^{NL} mice). We then created another line that also possessed the Beyreuther/Iberian mutation ($App^{NL\text{-}F}$ mice), although putting the two independent mutations together may potentially exert unexpected effects. The presence of intron 16 was indispensable for correct expression of APP (data not shown).

Wild-type ($App^{wt/wt}$), $App^{NL/NL}$ and $App^{NL\text{-}F/NL\text{-}F}$ mice generated equal amounts of APP and APP intracellular domain (AICD) (**Supplementary Fig. 3a,b**). Because Swedish mutations facilitate β-cleavage of APP[8], the levels of C-terminal fragment β (CTF-β) increased similarly in $App^{NL/NL}$ and $App^{NL\text{-}F/NL\text{-}F}$ mice in a gene dose–dependent manner. These observations indicate that $App^{NL/NL}$ mice are relevant negative controls for $App^{NL\text{-}F/NL\text{-}F}$ mice. In contrast, APP-Tg mice (APP23) produced much higher levels of APP, CTF-β/α and AICD than $App^{wt/wt}$ and $App^{NL\text{-}F/NL\text{-}F}$ mice (**Supplementary Fig. 4a**). The $App^{NL\text{-}F/NL\text{-}F}$ mice produced more $A\beta_{42}$ than any of the other mice; the ratio of $A\beta_{42}/A\beta_{40}$ was also highest in these mice (**Supplementary Fig. 4b–e**). The $A\beta_{42}$ levels increased in an age-dependent manner (**Fig. 1a**), accompanying progressive Aβ pathology (**Fig. 1b**). We detected initial deposition of Aβ at 6 months in the $App^{NL\text{-}F/NL\text{-}F}$ mice (**Supplementary Fig. 5**) and at 12 months in APP-Tg mice (**Supplementary Fig. 6a,b**). Heterozygous $App^{NL\text{-}F/wt}$ mice exhibited cortical amyloidosis only after 24 months (**Supplementary Fig. 7**).

We next investigated the N- and C-terminal structures of Aβ in the plaques of $App^{NL\text{-}F/NL\text{-}F}$ mice[9]. $A\beta_{1-42}$ appeared as an initial species, followed by $A\beta_{3(pE)-42}$ (**Fig. 1c** and **Supplementary Fig. 5**). $A\beta_{X-40}$ was a minor species. This observation, consistent with human pathology (**Supplementary Fig. 8a**), implies that conversion of $A\beta_{1-42}$ to $A\beta_{3(pE)-42}$ occurs after deposition of $A\beta_{1-42}$. In contrast, the APP-Tg mice mainly accumulated $A\beta_{1-40}$ (**Supplementary Fig. 6c**).

We observed accumulation of microglia and activated astrocytes (**Fig. 1d**), signs of neuroinflammation, around the Aβ plaques. We also detected synaptic alterations, as indicated by losses of synaptophysin and PSD95 immunoreactivities (**Fig. 1e**) similar to those observed in AD brains (**Supplementary Fig. 8b–d**). We then examined memory function in the $App^{NL\text{-}F/NL\text{-}F}$ mice using the Y-maze test (**Fig. 1f**). The mutant mice showed impairment at 18 months, whereas $App^{NL/NL}$ mice were normal. This suggests that the increase in CTF-β levels in the $App^{NL\text{-}F/NL\text{-}F}$ mice was not the cause of impairment, as $App^{NL\text{-}F/NL\text{-}F}$ and $App^{NL/NL}$ mice produce equal amounts of CTF-β (**Supplementary Fig. 3a,b**). However, extremely high levels of CTF-β may affect cognitive function in APP transgenic mice[10].

Deficiency in calpastatin augments AD-associated pathology in APP-Tg mice[11]. The most notable feature of the double mutant is early lethality: half of them die by 10 weeks. We had thus argued that the calpain-calpastatin system might have a major role in AD pathogenesis. To validate these phenotypes, we generated $App^{NL\text{-}F/NL\text{-}F}$ and $App^{NL/NL}$ mice that were deficient in calpastatin ($App^{NL\text{-}F/NL\text{-}F} \times Cast^{-/-}$ and $App^{NL/NL} \times Cast^{-/-}$). Calpastatin deficiency had no effect on the survival of $App^{NL\text{-}F/NL\text{-}F}$ and $App^{NL/NL}$ mice (**Supplementary Fig. 9a**). We also failed to reproduce other phenotypes such as increased tau phosphorylation and somatodendritic atrophy, as analyzed in a previously described manner[11] (data not shown). These are all likely artifacts caused by APP overexpression.

There were, however, a few confirmable phenotypes. Calpastatin deficiency exacerbated Aβ amyloidosis in the $App^{NL\text{-}F/NL\text{-}F}$ mice (**Supplementary Fig. 9b**), as in APP-Tg mice. We also observed concomitantly higher microgliosis and astrocytosis in $App^{NL\text{-}F/NL\text{-}F} \times Cast^{-/-}$ mice than in $App^{NL\text{-}F/NL\text{-}F}$ mice (**Supplementary Fig. 9c**). Calpastatin deficiency increased the biochemical levels of Aβ in $App^{NL\text{-}F/NL\text{-}F}$ mice, but not in $App^{NL/NL}$ mice (**Supplementary Fig. 9d**), suggesting that calpastatin deficiency affects processes associated with the deposition,

[1]Laboratory for Proteolytic Neuroscience, RIKEN Brain Science Institute, Wako-shi, Saitama, Japan. [2]Japan Science and Technology Agency, Saitama, Japan. [3]Laboratory for Behavioral Genetics, RIKEN Brain Science Institute, Wako-shi, Saitama, Japan. [4]Department of Molecular Medicinal Sciences, Division of Biotechnology, Nagasaki University Graduate School of Biomedical Sciences, Nagasaki, Japan. Correspondence should be addressed to T.C.S. (saido@brain.riken.jp).

Received 5 January; accepted 12 March; published online 13 April 2014; doi:10.1038/nn.3697

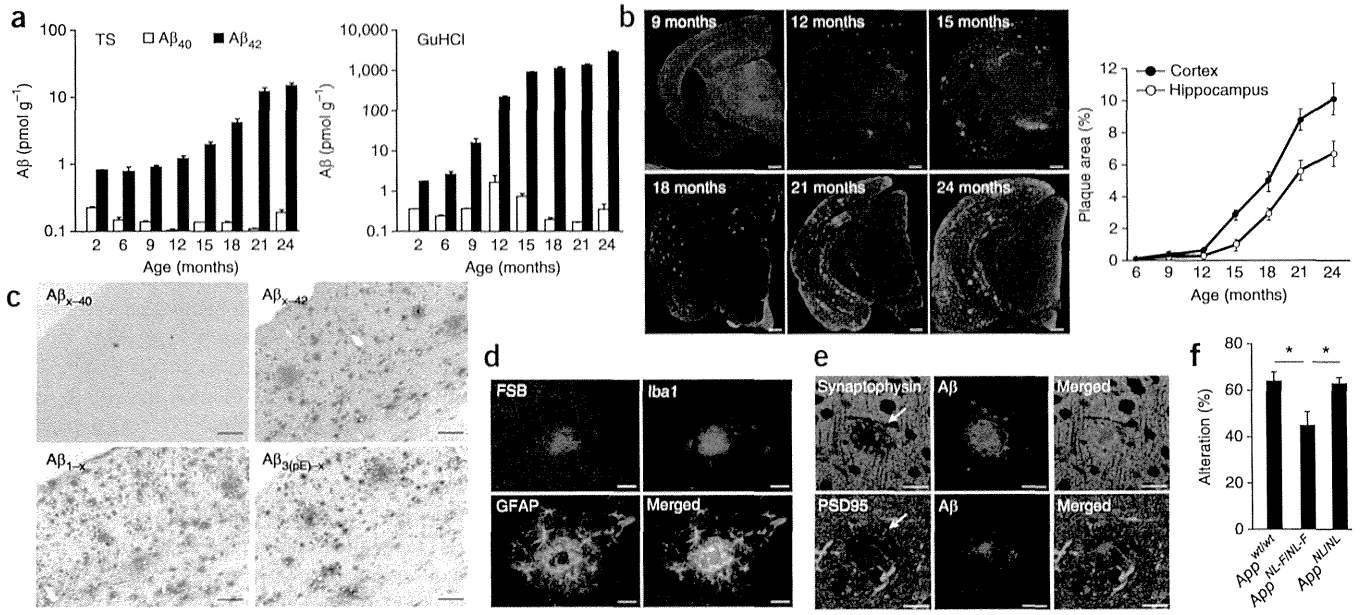

Figure 1 Neuropathology and memory impairment of $App^{NL\text{-}F/NL\text{-}F}$ mice. (**a**) Biochemical quantities of $A\beta_{40}$ and $A\beta_{42}$ in $App^{NL\text{-}F/NL\text{-}F}$ brains. Aβ levels in the Tris-HCl–buffered saline (TS) and GuHCl fractions of cortex from 2–24-month-old mice were quantified by sandwich ELISA. Data represent mean ± s.e.m. (n = 4, 4, 5, 6, 6, 6, 4 and 6 mice per indicated time point, respectively). (**b**) Aβ pathology in $App^{NL\text{-}F/NL\text{-}F}$ brains. Brain sections from 9–24-month-old $APP^{NL\text{-}F/NL\text{-}F}$ mice were immunostained with antibody to Aβ (4G8). Plaque areas were quantified as indicated in the graph on the right (n = 4, 5, 6, 6, 6, 4 and 6 mice per indicated time point, respectively). Scale bars represent 500 μm. (**c**) N- and C-terminal structures of Aβ in the $App^{NL\text{-}F/NL\text{-}F}$ brain. Brain sections from 24-month-old $App^{NL\text{-}F/NL\text{-}F}$ mice (n = 4) were immunostained with endo-specific antibodies as indicated. Scale bars represent 100 μm. (**d**) Neuroinflammation in $App^{NL\text{-}F/NL\text{-}F}$ mouse brains. Inflammatory responses were detected by triple staining using fluorostyryl benzene (FSB), antibody to GFAP and antibody to Iba1 as markers of cored Aβ plaque, astrocytosis and microgliosis, respectively. Cortical immunoreactivities were quantified as shown in **Supplementary Figure 3c**. Scale bars represent 25 μm. (**e**) Synaptic alterations in $App^{NL\text{-}F/NL\text{-}F}$ mouse brains. Double staining was performed using 4G8 antibody with a presynaptic marker (antibody to synaptophysin) and with a postsynaptic marker (antibody to PSD95). Scale bars represent 10 μm. (**f**) Memory impairment in $App^{NL\text{-}F/NL\text{-}F}$ knock-in mice. The Y-maze test was performed using 18-month-old mice. Data represent mean ± s.e.m. (n = 10, one-way ANOVA with Sheffe's F test, $^*P < 0.05$).

rather than the generation, of Aβ. Furthermore, calpastatin deficiency increased the memory impairment of $App^{NL\text{-}F/NL\text{-}F}$ mice by 3 months (**Supplementary Fig. 9e**), consistent with accelerated Aβ pathology.

Some of the phenotypes that we observed in APP-Tg mice therefore turned out to be artifacts, presumably resulting from high levels of APP and non-Aβ fragments, whereas other phenotypes did not. This makes $App^{NL\text{-}F/NL\text{-}F}$ mice convenient tools for distinguishing facts from artifacts in the phenotypes thus far reported using APP-Tg mice crossbred with other genetically modified mice. In particular, the roles of tau[12] and apolipoprotein E[13] are important. It is also possible that some of the clinical trials of candidate AD therapeutics failed because the researchers immediately progressed from APP-Tg mice to humans without any additional validation.

We also generated another line of mice that carry the Arctic mutation[14,15] in addition to the Swedish and Beyreuther/Iberian mutations ($App^{NL\text{-}G\text{-}F}$) (**Supplementary Fig. 1b**). $App^{NL\text{-}G\text{-}F/NL\text{-}G\text{-}F}$ mice exhibited APP expression and processing identical to that of $App^{NL\text{-}F/NL\text{-}F}$ mice (**Supplementary Fig. 10a,b**). However, this mutation, located in the middle of the Aβ sequence, altered the binding properties of various antibodies to Aβ, as analyzed by sandwich ELISA and immunohistochemistry (**Supplementary Fig. 11**). Antibodies to the N and C termini appeared to bind to both Aβ species in a similar manner. Using an appropriate combination of the antibodies, we observed aggressive Aβ amyloidosis in $App^{NL\text{-}G\text{-}F/NL\text{-}G\text{-}F}$ mice in an age-dependent manner (**Fig. 2a,b**). Notably, the cortical deposition began by 2 months and was almost saturated by 7 months. The heterozygous mice began Aβ deposition at 4 months (**Supplementary Fig. 12**).

Unlike $App^{NL\text{-}F/NL\text{-}F}$ mice, $App^{NL\text{-}G\text{-}F/NL\text{-}G\text{-}F}$ mice also showed subcortical amyloidosis after 4 months (**Fig. 3b**), consistent with the pathology of human Arctic mutation carriers[16]. This subcortical amyloidosis was not detected in mice overexpressing human APP with the Arctic mutation, presumably because an artificial promoter was used to drive the transgene expression[17]. We observed greater microgliosis and astrocytosis in 9-month-old $App^{NL\text{-}G\text{-}F/NL\text{-}G\text{-}F}$ mice than in 18-month-old $App^{NL\text{-}F/NL\text{-}F}$ mice (**Fig. 2c**), implying that the Arctic Aβ may be more proinflammatory than wild-type Aβ. The reduction in synaptophysin and PSD95 immunoreactivities near Aβ plaques was similar in these mutant mice (**Figs. 1e** and **2d**). Consistent with the pronounced Aβ pathology, $App^{NL\text{-}G\text{-}F/NL\text{-}G\text{-}F}$ mice showed memory impairment by 6 months (**Fig. 2e**), approximately three times faster than $App^{NL\text{-}F/NL\text{-}F}$ mice.

The memory impairment that we observed in our mutant mice is likely to reflect preclinical cognitive decline in humans[18]. We therefore consider these mice to be useful tools for identifying and validating pathways by which Aβ amyloidosis induces subsequent pathological changes. A number of approaches can now be adopted, including pathway analyses based on various 'omics' data. We can also analyze the tau interactome to identify protein(s) that may link Aβ amyloidosis and tauopathy. In any case, the advantages lie in the existence of relevant negative controls and the lack of concern about overexpression artifact(s).

$App^{NL\text{-}F/NL\text{-}F}$ mice will also provide a better tool for identifying upstream factors that affect Aβ amyloidosis than $App^{NL\text{-}G\text{-}F/NL\text{-}G\text{-}F}$ mice, given that the sequence of Aβ is identical to that of wild-type Aβ, which accumulates in most familial and sporadic AD patients.

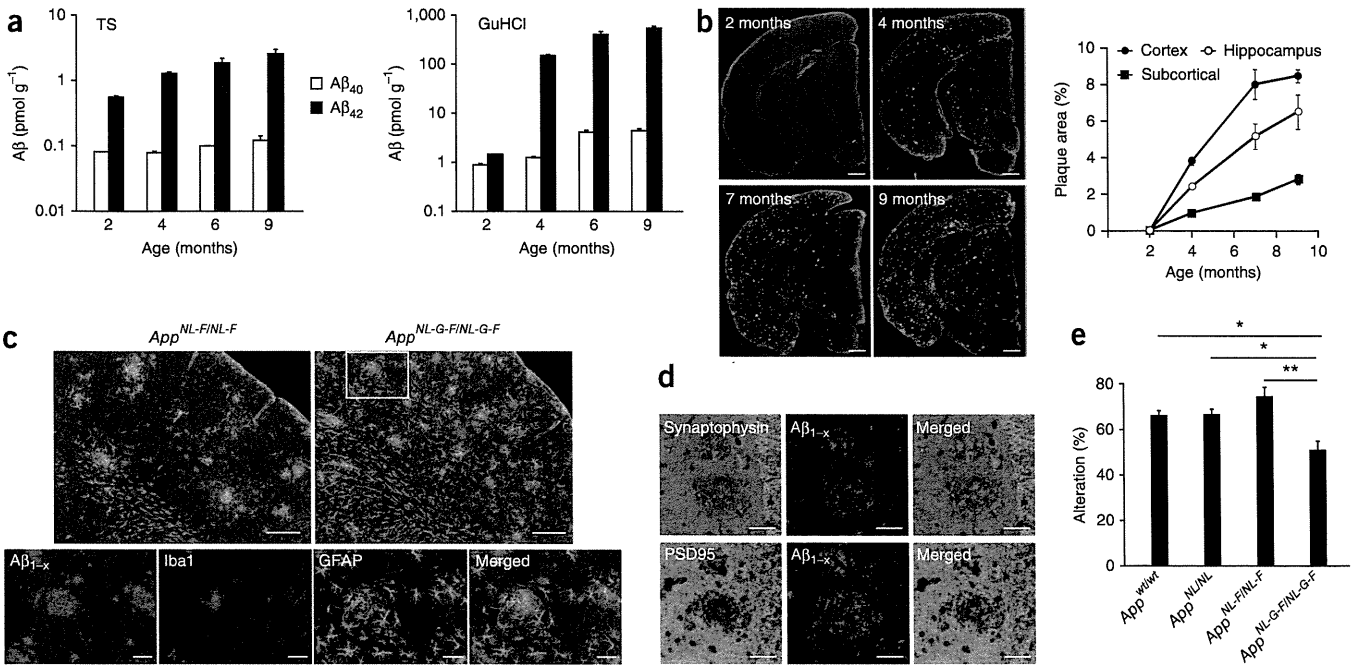

Figure 2 Neuropathology and memory impairment of $App^{NL\text{-}G\text{-}F/NL\text{-}G\text{-}F}$ mice. (**a**) Biochemical quantities of Aβ in $App^{NL\text{-}G\text{-}F/NL\text{-}G\text{-}F}$ brains. We quantified $Aβ_{40}$ and $Aβ_{42}$ in the TS and GuHCl fractions of cortex from 2–9-month-old mice by sandwich ELISA. We generated standard curves for calibration using synthetic $Aβ_{1\text{–}40}$ and $Aβ_{1\text{–}42}$ with E22G amino acid replacement (**Supplementary Fig. 11**). Data represent mean ± s.e.m. (n = 4, 4, 6 and 6 mice per indicated time point, respectively). (**b**) Aβ deposition in $App^{NL\text{-}G\text{-}F/NL\text{-}G\text{-}F}$ brains. Brain sections from 2–9-month-old $App^{NL\text{-}G\text{-}F/NL\text{-}G\text{-}F}$ mice were immunostained using antibody to $Aβ_{42}$. Cortical, hippocampal and subcortical immunoreactive plaque areas were quantified as shown in the graph on the right (n = 3, 3, 4 and 4 mice per indicated time point, respectively). Scale bars represent 500 μm. (**c**) Neuroinflammation in $App^{NL\text{-}G\text{-}F/NL\text{-}G\text{-}F}$ mouse brains. Inflammatory responses were detected by triple staining of frozen sections from 18-month-old $App^{NL\text{-}F/NL\text{-}F}$ mice and from 9-month-old $App^{NL\text{-}G\text{-}F/NL\text{-}G\text{-}F}$ mice. Bottom, superimposed images of the boxed area in the upper right panel ($App^{NL\text{-}G\text{-}F/NL\text{-}G\text{-}F}$ mice) at a higher magnification. Cortical immunoreactivities were quantified as shown in **Supplementary Figure 10a**. Scale bars represent 100 μm (top) and 25 μm (bottom). (**d**) Synaptic alterations in $App^{NL\text{-}G\text{-}F/NL\text{-}G\text{-}F}$ mouse brains. Double staining was performed using antibody to $Aβ_{1\text{–}x}$ with antibodies to synaptophysin and PSD95. Scale bars represent 10 μm. (**e**) Memory impairment in $App^{NL\text{-}G\text{-}F/NL\text{-}G\text{-}F}$ mice. The Y-maze test was performed using 6-month-old mice. Data represent mean ± s.e.m. (n = 10 $App^{wt/wt}$, 9 $App^{NL/NL}$, 9 $App^{NL\text{-}F/NL\text{-}F}$ and 10 $App^{NL\text{-}G\text{-}F/NL\text{-}G\text{-}F}$, one-way ANOVA with Sheffe's F test, $^{*}P < 0.05$ and $^{**}P < 0.01$).

It will be interesting to examine the phenotypes of $App^{NL\text{-}F/NL\text{-}F}$ mice lacking autophagosomal function, as Atg7 deficiency induces impairment of Aβ secretion, accumulation of intracellular Aβ and neurodegeneration with no sign of tauopathy[19], implying the presence of pathway(s) that lead from intracellular Aβ to neurodegeneration independent of tauopathy. On the basis of these facts and assumptions, we propose that $App^{NL\text{-}F/NL\text{-}F}$ and $App^{NL\text{-}G\text{-}F/NL\text{-}G\text{-}F}$ mice be used as standard mouse models for identifying mechanisms and pathways upstream and downstream of Aβ amyloidosis.

METHODS

Methods and any associated references are available in the online version of the paper.

Note: Any Supplementary Information and Source Data files are available in the online version of the paper.

ACKNOWLEDGMENTS

We thank C.A. Lemere (Brigham and Woman's Hospital) and M. Higuchi (National Institute of Radiological Science) for valuable discussions. We also thank E. Takano, R. Fujioka and Y. Tomita for technical assistance. This work was supported by research grants from RIKEN Brain Science Institute, the Ministry of Education, Culture, Sports, Science and Technology, the Ministry of Health and Welfare, grants-in-aid for the Molecular Imaging Program, Japan Science and Technology Agency Precursory Research for Embryonic Science and Technology, the Cell Science Research Foundation and the Takeda Science Foundation.

AUTHOR CONTRIBUTIONS

This study was designed by T.S. and T.C.S. Generation of the knock-in mice was supported by S.I. Experiments were performed by T.S., Y.M., N.M. and J.T. T.S., J.T., P.N., N.I. and T.C.S. jointly analyzed and interpreted data.

COMPETING FINANCIAL INTERESTS

The authors declare competing financial interests: details are available in the online version of the paper.

1. Jonsson, T. *et al. Nature* **488**, 96–99 (2012).
2. Hardy, J. & Allsop, D. *Trends Pharmacol. Sci.* **12**, 383–388 (1991).
3. Hsiao, K. *et al. Science* **274**, 99–102 (1996).
4. Sturchler-Pierrat, C. *et al. Proc. Natl. Acad. Sci. USA* **94**, 13287–13292 (1997).
5. Citron, M. *et al. Nature* **360**, 672–674 (1992).
6. Lichtenthaler, S.F. *et al. Proc. Natl. Acad. Sci. USA* **96**, 3053–3058 (1999).
7. Guardia-Laguarta, C. *et al. J. Neuropathol. Exp. Neurol.* **69**, 53–59 (2010).
8. Forman, M.S. *et al. J. Biol. Chem.* **272**, 32247–32253 (1997).
9. Saido, T.C. *et al. Neuron* **14**, 457–466 (1995).
10. Mitani, Y. *et al. J. Neurosci.* **32**, 2037–2050 (2012).
11. Higuchi, M. *et al. FASEB J.* **26**, 1204–1217 (2012).
12. Roberson, E.D. *et al. Science* **316**, 750–754 (2007).
13. Liu, C.C., Kanekiyo, T., Xu, H. & Bu, G. *Nat. Rev. Neurol.* **9**, 106–118 (2013).
14. Hashimoto, T. *et al. J. Biol. Chem.* **286**, 27081–27091 (2011).
15. Tsubuki, S., Takaki, Y. & Saido, T.C. *Lancet* **361**, 1957–1958 (2003).
16. Kalimo, H. *et al. Acta Neuropathol. Commun.* **1**, 60 (2013).
17. Cheng, I.H. *et al. Nat. Med.* **10**, 1190–1192 (2004).
18. Cash, D.M. *et al. Neurology* **81**, 1425–1433 (2013).
19. Nilsson, P. *et al. Cell Reports* **5**, 61–69 (2013).

ONLINE METHODS

Generation of $App^{NL/NL}$, $App^{NL\text{-}F/NL\text{-}F}$ and $App^{NL\text{-}G\text{-}F/NL\text{-}G\text{-}F}$ mice. As described in **Supplementary Figure 1**, we isolated mouse *App* genomic DNA from the bacterial artificial chromosome (BAC) library carrying the C57BL/6 mouse genome, which included introns 15–17. We humanized the Aβ sequence and introduced Swedish mutations into exon 16, and Beyreuther/Iberian and Arctic mutations into exon 17. Finally, we inserted a *pgk-neo* gene cassette with a lox/FRT sequence in intron 16 for positive selection. We used the fragment spanning intron 15 to exon 16 (genomic mouse *App* from 206,484 to 207,984; approximately 1.5 kbp) and the fragment spanning exon 17 to intron 17 (genomic mouse *App* from 210,922 to 216,617; approximately 5.7 kbp) as the short-arm and long-arm targeting vectors, respectively.

Embryonic stem (ES) cell culture and gene targeting were carried out as previously described[20]. Targeted ES cells were microinjected into C57BL/6 blastocysts. We extracted DNA from the biopsied tails of mouse pups and identified the F1 generation by Southern blotting using the following 5′ and 3′ external probes. The former was generated by PCR using a primer pair of 5′-ACCTGTTCCAATAACTCTACAGCC-3′ and 5′-ATGTGGCAGTGACATGAATGCTC-3′, and the latter by 5′-CACTCA CAGTCATTCACAGTGC-3′ and 5′-GGCATCTACTTGTGTTACAGCAC-3′.

We then crossbred heterozygous mutant mice with EIIa-Cre Tg mice to remove the *pgk-neo* gene. Finally, we removed the EIIa-Cre transgene by crossing the mice with wild-type C57BL/6 mice. We genotyped the mice by PCR using the following cocktail of primers: 5′-ATCTCGGAAGTGAAGATG-3′, 5′-ATCTCGGAAGTGAATCTA-3′, 5′-TGTAGATGAGAACTTAAC-3′ and 5′-CGTATAATGTATGCTATACGAAG-3′.

Other mutant mice. APP23 mice, which overexpress Swedish mutation–containing human APP751 under the control of the neuron-specific Thy-1 promoter, were maintained as previously described[4]. Calpastatin knockout ($Cast^{-/-}$) mice have also been described previously[20]. All the mice used in the experiments were on the C57BL/6J background. All animal experiments were carried out according to the RIKEN Brain Science Institute's guidelines for animal experimentation.

Northern blot analysis. Total RNA from brain tissues were subjected to northern blotting to quantify APP expression levels using a North2South labeling and detection kit (Thermo Scientific), according to the manufacturer's instructions. Specific probes to identify the RNA of mouse *App* and *Actb* were produced by PCR using the following primer pairs: 5′-ATGTGCAGAATGGAAAGT-3′ and 5′-CAGCATACAAACTCTACC-3′ for the former, and 5′-TCATGAAGTGTG ACGTTGACATCCGT-3′ and 5′-CTTAGAAGCATTTGCGGTGCACGATG-3′ for the latter. Full-length blots for this experiment are shown in **Supplementary Figure 13**.

Western blot analysis of APP and APP-derived fragments. Brain homogenates prepared as previously described[21] were subjected to western blotting using antibody to human $Aβ_{1-12}$ (6E10, Covance), antibody to APP N terminus (22C11, Millipore) and antibody to APP-CTF (A8717, Sigma). Each set of experiments was repeated at least three times to confirm the results. The band intensity was determined with a densitometer, LAS4000 (Fujifilm). Full-length blots for these experiments are shown in **Supplementary Figure 14**.

Enzyme-linked immunosorbent assay (ELISA). Soluble materials from mouse cortical hemispheres were dissolved in TS fraction and insoluble materials in guanidine-HCl solution (GuHCl fraction) as previously described[22]. We quantified $Aβ_{X-40}$ and $Aβ_{X-42}$ in these fractions using an Aβ ELISA kit (Wako) according to the manufacturer's instructions. We quantified $Aβ_{X-40}$ and $Aβ_{X-42}$ carrying the Arctic mutation based on standard curves using synthetic human Arctic Aβ peptides (Peptide Institute).

Immunohistochemical and histochemical studies. We immunostained paraffin-embedded and frozen mouse brain sections using antibodies specific to the N termini of Aβ ($Aβ_{1-X}$ and $Aβ_{3(pE)-X}$[9]), the N-terminal region of Aβ (82E1, IBL), $Aβ_{17-24}$ (4G8, Covance), $Aβ_{X-40}$ (IBL), $Aβ_{X-42}$ (IBL), phosphorylated tau (AT8, Invitrogen), synaptophysin (conjugated with FITC; clone SY38, PROGEN), the PSD95 PDZ domain (Synaptic Systems), Iba1 (Wako) and GFAP (MAB3402, Millipore). We used tyramide signal amplification (PerkinElmer Life Sciences), when necessary, as previously described[23]. 1-fluoro-2,5-bis(3-carboxy-4-hydroxystyryl)benzene (FSB) was used for detection of amyloidosis[11]. We performed antigen retrieval by autoclave (121 °C for 5 min) for 82E1 and 6E10 staining or by formic acid treatment (90% formic acid for 5 min at 20–25 °C) for immunohistochemistry of 4G8, $Aβ_{X-40}$ and $Aβ_{X-42}$ antibodies. We quantified the immunoreactive areas using MetaMorph imaging software (Universal Imaging) as previously described[23]. To reduce the variance among tissue sections, we used the average of data from at least four sections per mouse as an individual value.

Y-maze and Morris water maze tests. The Y-maze test was performed with a slight modification as previously described[24]. Mice were caged in a group of three to five individuals before transferring to a behavioral laboratory. The light condition was 12-h:12-h (lights on 8:00). All of the experiments were conducted in the light phase (9:00–18:00), and the starting time of the experiments was kept constant.

The Y-maze apparatus (O'Hara & Co), made of gray plastic, consisted of three compartments (3 cm (W) bottom and 10 cm (W) top, 40 cm (L) and 12 cm (H)) radiating out from the center platform (3 × 3 × 3 cm triangle), and positioned 60 cm above the floor. In this test, each mouse was placed in the center of the maze facing toward one of the arms and then allowed to explore freely for 5 min. The light intensity of the platform was kept at 80 lx. We recorded and analyzed the activity and spontaneous behavioral alternations of the mice using Time YM2 for Y-maze (Two Maze System, O'Hara & Co). A reduction in the behavioral alternations corresponds to memory impairment[25].

The Morris water maze test was performed as previously described[19], with minor modifications using Time MWM for the Morris water maze (O'Hara & Co). Although a tendency toward memory impairment was detected in 18-month-old $App^{NL\text{-}F/NL\text{-}F}$ mice, it did not reach statistical significance ($P = 0.893$; data not shown).

AD brain sections. Postmortem AD brain tissues were kindly provided by J.Q. Trojanowski and V.M.-Y. Lee (University of Pennsylvania). The tissues had been fixed with ethanol or formalin and embedded in paraffin. Paraffin-embedded brain (neocortical and hippocampal region) sections from normal humans and AD patients were also purchased from Wako (Japan). The research plans to use human materials were approved by the Institutional Review Board of the RIKEN Brain Science Institute.

Statistical analysis. All data are shown as mean ± s.e.m. For comparison between two groups, statistical analysis was performed by Student *t* test. For comparisons among three or more groups, we used one-way analysis of variance (ANOVA) or repeated-measures ANOVA followed by *post hoc* test (Scheffe *F* test). Normality was tested using Statcel 3 (add-in software for Excel, Microsoft). The data were collected and processed in a randomized and blinded manner. No statistical methods were used to predetermine sample size, but our sample sizes were similar to those generally employed in the field.

20. Takano, J. *et al. J. Biol. Chem.* **280**, 16175–16184 (2005).
21. Saito, T. *et al. Nat. Med.* **11**, 434–439 (2005).
22. Iwata, N. *et al. J. Neurosci.* **24**, 991–998 (2004).
23. Enya, M. *et al. Am. J. Pathol.* **154**, 271–279 (1999).
24. Saito, T. *et al. Nat. Neurosci.* **14**, 1023–1032 (2011).
25. Sarnyai, Z. *et al. Proc. Natl. Acad. Sci. USA* **97**, 14731–14736 (2000).